Volume 373 1 January 2007 ISSN 0378-4371

PHYSICA A
STATISTICAL MECHANICS AND ITS APPLICATIONS
Recognized by the European Physical Society

Complete Volume

Available online at
ScienceDirect
www.sciencedirect.com
http://www.elsevier.com/locate/physa

Available online at www.sciencedirect.com
ScienceDirect
Physica A 373 (2007) 455–476
PHYSICA A
www.elsevier.com/locate/physa

Molecular dynamics study of structural properties of β-sheet assemblies formed by synthetic de novo oligopeptides

Giovanni Bellesia[a,*], Maxim V. Fedorov[b,1], Edward G. Timoshenko[c]

[a]School of Chemistry and Chemical Biology, Science Centre South, University College Dublin, Belfield, Dublin 4, Ireland
[b]Centre for Synthesis and Chemical Biology, School of Chemistry and Chemical Biology, Science Centre South, University College Dublin, Belfield, Dublin 4, Ireland
[c]Laboratory of Biomolecular Conformations, Centre for Synthesis and Chemical Biology, Conway Institute of Biomolecular and Biomedical Research, School of Chemistry and Chemical Biology, Science Centre South, University College Dublin, Belfield, Dublin 4, Ireland

Received 1 June 2006
Available online 10 July 2006

Abstract

We study, by means of molecular dynamics (MD) simulations with explicit water, the structure and stability of β-sheet tapes, ribbons and double ribbons formed by rationally designed oligopeptides P_{11}-I and P_{11}-II in aqueous solutions. Two different methods for the treatment of the electrostatic interactions were considered: a smoothly shifted spherical cutoff approach under spherical harmonic conditions, and the particle mesh Ewald technique.

We investigate the transfer of chirality from single L-aminoacids to the molecular scale of oligopeptides and from the latter to the supramolecular scale of peptide clusters. Furthermore, we obtain structural data for the representative conformations of these clusters, as well as study various average properties of their geometry.

Keywords: Peptide-based clusters; Supramolecular chirality; Molecular dynamics

1. Introduction

Low-cost techniques for peptide synthesis developed in recent years [1] have stimulated interest to the self-assembly of synthetic oligopeptides as a route towards novel biomaterials [2–4].

Peptide-based assemblies have many applications ranging from 3D-scaffolding for tissue growth, biochips and drug delivery, to nanomachinery [2–6]. There is considerable similarity between the mechanisms of self-assembly of these oligopeptides and amyloid plaque formation [7].

*Corresponding author. Current address: Department of Chemistry and Biochemistry, University of California Santa Barbara, CA 93106-9510, USA.
E-mail addresses: gbellesia@chem.ucsb.edu (G. Bellesia), mvf22@cam.ac.uk (M.V. Fedorov), edward.timoshenko@ucd.ie (E.G. Timoshenko).
[1]Current address: Unilever Centre For Molecular Science Informatics, Department of Chemistry, University of Cambridge, Lensfield Road, Cambridge, CB2 1EW, UK.

0378-4371/$ - see front matter © 2006 Elsevier B.V. All rights reserved.
doi:10.1016/j.physa.2006.06.011

It is well known that certain oligopeptides are capable of self-assembly in solution into β-sheet semiflexible tapes, which was demonstrated by a number of experimental studies [2–4,8–11]. Among others, P_{11}-I and P_{11}-II [13,9,1] oligopeptides are good examples of molecules producing a rich variety of structures.

In aqueous solution of these oligopeptides a hierarchy of equilibrium structures emerges as a function of the peptide concentration: helicoid antiparallel β-tapes, double tapes (ribbons), fibrils and fibres. Even at fairly low concentrations, ($c \geqslant 4$ mM), these become entangled and yield nematic solutions [14], further producing self-supporting thermostable nematic gels.

The primary structure of P_{11}-I peptide is CH3–CO–QQRQQQQQEQQ–NH2. Hydrophobic interactions are provided by the $(–CH_2–)_2$ moieties in the Glutamine (Q) side-chains. Arginine (R) and Glutamic acid (E) in symmetric positions add strong Coulombic attractions towards the antiparallel pattern. These, and the hydrogen bonding, thus result in the β-sheet tape structures.

Peptide P_{11}-II has the primary structure CH3–CO–QQRFQWQFEQQ–NH2 and was specifically designed from peptide P_{11}-I in order to increase the tendency of ribbon formation. Glutamine residues in positions 4,6 and, 8 are thus replaced by Phenylalanine (F), Tryptophan (W) and another Phenylalanine respectively, which supply hydrophobic interactions as well as additional intermolecular recognition via π–π interaction. The amphiphilic nature of the P_{11}-II peptide facilitates formation of β-tapes, and the hydrophobic side, (QFWFQ), promotes formation of ribbons in water solution.

Search for the detailed geometry of these β-tapes, ribbons, fibrils and fibers is being limited by their non-crystalline nature and large size. Consequently, both X-ray spectroscopy and solution-phase NMR cannot be used here readily. Therefore, until now, experimental analysis has been restricted to the techniques of Fourier transform infrared spectroscopy (FTIR), ultra-violet circular dichroism (UV–CD) and transmission electron microscopy (TEM) [1]. FTIR and UV–CD analyses indicate that the supramolecular structures are formed by antiparallel β-sheets. TEM micrographs show that those structures are of a chiral nature and characterized by a stable left-handed twist.

The *microscopic* chirality of amino acids leads to the *mesoscopic* chirality of the β-sheet tape, and likewise to that of the ribbons and the fibrils, resulting in a finite twist of the β-sheet self-assemblies, similar to that of β-sheet motifs in globular proteins [15–22].

Moreover, handedness at the oligopeptide scale causes a favorable *packing orientation* between adjacent β-strands [23]. As a result, a finite *twist angle* between neighboring strands can be observed and the supramolecular cluster grows as a chiral structure as well. Indeed, as a consequence of the strand right-handed twist, the β-tapes as well as the ribbons and fibrils formed by P_{11}-I and P_{11}-II peptides are left-handed about the axis normal to the peptides chains (we shall call the former the principal axis of the tape, ribbon, and fibril) [15,18,1].

Therefore, chirality is firstly *transferred* from the single amino acids to the greater molecular scale of the β-strands and secondly from the single β-strands to the greater supramolecular scale of the β-tapes, ribbons and fibrils [24].

Until now, there were few simulation studies on supramolecular peptide-based assemblies, such as β-tapes and ribbons (double tapes), using MD at the atomistic level [10–12,25]. The stability of those clusters was investigated (under periodic boundary conditions) over simulation times stemming from hundreds of picoseconds [10,11,25] to several nanoseconds [12]. Both explicit [12] and implicit solvent [10,11,25] Hamiltonians were used in those studies as well as the spherical cutoff method [12] and the PME method [10,11,25] for the treatment of the electrostatic interactions.

In particular, MD simulations of tapes and ribbons formed by peptides P_{11}-I and P_{11}-II were carried out by Fishwick et al. [25]. The authors investigate some structural features of those clusters over a timelength of 100 ps. First, the simulations indicate that the antiparallel β-sheet orientation of tapes and ribbons is the most stable for both peptides, thereby confirming the experimental results (FTIR and CD spectra) [1]. Second, the final geometries of the clusters are in qualitative agreement with what observed in TEM micrographs analysis.

In our study, we extend the analysis on the structures formed by peptides P_{11}-I and P_{11}-II to tapes, ribbons and double ribbons over simulation times of several nanoseconds using explicit solvent and two different treatments for the long-range ES interactions. The geometry and stability of all the structures have been assessed by defining a consistent set of structural parameters as well as by calculating both their averages values and the corresponding fluctuations.

Results from our work (see Section 3) show that all the structures are stable over simulation times of several nanoseconds and that their geometry is in good agreement with the experimental observations.

We found that the structural stability increases with the complexity of the clusters (from tape to ribbons and from ribbons to double ribbons) and that it mainly depends on short-range forces. In particular, ribbons and double ribbons display a solid-like structural order.

Furthermore, we defined a molecular chiral parameter and showed that its value is consistently coupled (in sign and magnitude) to the *macroscopic* chirality of the clusters.

As mentioned previously, current experimental studies of these supramolecular structures have, by necessity, been relatively low-resolution in nature. Hence, the atomistic description of the systems carried out in this paper may facilitate future studies on different physical–chemical factors governing the stability of the peptide assemblies such as pH, temperature and ionic strength.

2. Materials and methods

Experimental results [1] together with findings from previous MD simulations [25] (see Section 1) were considered in the choice of the starting configurations for our computational study.

In silico models of the peptides P_{11}-I and P_{11}-II in a fully-extended β-strand conformation were generated using HyperChem(TM) software [26].

Single tapes were produced by "manually" placing $N = 20$ peptides into a planar, antiparallel-like arrangement [1,25]. Flat double tapes (ribbons) and double ribbons were then obtained by assembling 2 and 4 planar tapes, respectively. Moreover, for both P_{11}-I and P_{11}-II, the ribbons were set up such that they had identical (polar) outer faces comprising Glutamine residues in positions 1, 5, 7 and 11, as well as Arginine and Glutamic acid residues. It should be also noted that both the ribbons and the double ribbons were assembled with the relative position of the neighboring layers (tapes) being antiparallel [1,25].

2.1. Procedure for MD simulations

For the simulations, the NAMD [27,28] software was used, with the CHARMM [29] force field. Six different systems were considered in this study (see Table 1 for details).

The first step in the computational procedure was the minimization of the potential energy of each structure (in vacuo) by using a version of the steepest descent algorithm [27,28]. At the end of this first step all the structures already resemble chiral β-sheet aggregates.

In the second step, each minimized structure was enclosed in a water sphere by adding explicit water molecules based on the TIP3P model. The value of the sphere radius was chosen such that there was a minimum water shell of 10 Å surrounding the peptide-based cluster [30].

The geometries obtained from a second energy minimization of those solvated systems were used as the initial conformations for a *first set* of MD simulations.

Table 1
Summary of the systems considered in the molecular dynamics simulations

Systems					
Cluster	Sequence	No. of atoms	No. of peptides	No. of layers	Name
Tape	P_{11}-I	4020	20	1	TP1
Ribbon	P_{11}-I	8040	40	2	RP1
Double ribbon	P_{11}-I	16080	80	4	DP1
Tape	P_{11}-II	4280	20	1	TP2
Ribbon	P_{11}-II	8560	40	2	RP2
Double ribbon	P_{11}-II	17120	80	4	DP2

Integration of the Newton's equations of motion was performed by using the velocity Verlet algorithm with a timestep of 2 fs. The bonds between hydrogens and the heavier atoms were constrained to their nominal lengths during integration by using the RATTLE algorithm [31]. The temperature was maintained at 300 K by coupling the system to a heat bath via the Berendsen thermostat [32].

The spherical harmonic boundary conditions (SHBC) were applied both in the energy minimization and in the first set of MD simulations of the solvated peptide-based supramolecular clusters. The simulation times, for the MD runs under SHBC, varied from 16 to 20 ns for each system. A good equilibration of the structures was achieved after 12–16 ns, correspondingly.

In more detail, the SHBC were enforced by means of a single potential function:

$$E_{\text{sphere}} = \begin{cases} k_{\text{sphere}}(|\mathbf{r}_i - \mathbf{r}_{\text{centre}}| - r_{\text{sphere}})^2 & \text{if } |\mathbf{r}_i - \mathbf{r}_{\text{centre}}| > r_{\text{sphere}}, \\ 0 & \text{otherwise,} \end{cases}$$

where $k_{\text{sphere}} = 10\,\text{kcal/mol}$, $\vec{r}_i$ the current position of an atom i, $\mathbf{r}_{\text{center}}$ the center of the water sphere and r_{sphere} the radius of the water sphere. In all our molecular simulations, the contribution of this 'boundary potential' was found to be negligible if compared to the total potential energy of the system (cluster + water molecules), i.e., less than 0.1% of the total potential energy in all cases.

In a recent paper, Beck et al. [33] have explored the use of different spherical cut-off approaches for the correct treatment of the long-range forces for solvated polypeptides. The authors show that, when both the electrostatic and van der Waals (Lennard-Jones) terms are smoothly shifted, the force-shifted spherical cut-off method correctly predicts the experimental *helicity content* (structural parameter) of the short peptide analyzed in their study. Moreover, there is a convergence in the simulations statistics as the cut-off is increased beyond 8 Å.

Another study by Garemyr and Elofsson [34] has showed that increasing the cut-off beyond 8 Å does not significantly improve the accuracy of molecular simulations for *Escherichia coli* thioredoxin.

In our simulations under SHBC we follow a similar approach, i.e., both the electrostatic and the van der Waals potential terms are smoothly shifted (by using polynomial functions), so that they are equal to zero at the cut-off distance of 8 Å.

Further, the six *representative structures* (see Section 3 for details) generated from the MD simulations under SHBC were used as initial coordinates for an additional *second set* of MD simulations under periodic boundary conditions (PBC). Each representative structure was enclosed in a water box whose dimensions were chosen such that there was a minimum water shell, varying from 10 Å (systems RP1, RP2, DP1 and DP2) to 15 Å (systems TP1 and TP2), surrounding the peptide-based cluster. Long-range electrostatic interactions were calculated by using the Ewald summation method [35,36] with the particle mesh Ewald (PME) algorithm [36]. The cut-off distance for the calculation of the electrostatic interactions in the direct space was 8 Å, while the accuracy was fixed at 10^{-6}, the order of the interpolation functions on the grid was set to 4 (cubic) and the grid size was $\sim$1 Å.

We have obtained a good convergence for the main structural observables after 2–4 ns. Subsequently, each production run lasted 4 ns.

Results from MD simulations under PBC extend our computational study on β-sheet peptide clusters, for which high-resolution experimental data are not as yet available. Furthermore, as the choice of the most appropriate electrostatic treatment (in terms of accuracy/CPU time) in molecular simulations of solvated biomolecules is still under debate [33,36–38], a comparison of the two methods (i.e., spherical cut-off and PME) is useful for gaining a better insight into the structural properties of the supramolecular structures of interest.

2.2. Definitions

The handedness and the magnitude of the local twist within the lth layer of ith β-strand can be explicitly quantified by calculating the value of the dihedral angles $\theta_i^l(n)$ defined by the quadruplets $C_\beta^i(n) - C_\alpha^i(n) - C_\alpha^i(n+2) - C_\beta^i(n+2)$. Note that in this definition we skip two positions in n so that C_β

atoms are on the same side. Right-handed and left-handed twists are associated with positive and negative values of $\theta_i^l(n)$, respectively [21].

The pitch wave number (local twist angle between two neighboring β-strands) within layer l has been calculated from the following formula:

$$k_{i,i+1}^l = \mathrm{sign}(LDA) \cdot \arccos\left(-\frac{\mathbf{x}_{ii}}{\|\mathbf{x}_{ii}\|} \cdot \frac{\mathbf{x}_{i+1,i+1}}{\|\mathbf{x}_{i+1,i+1}\|}\right), \tag{1}$$

where $\mathbf{x}_{ij} = (C_\alpha^i(Q5) - C_\alpha^j(Q7))$, with $Q5$ and $Q7$ referring to the Glutamine residues in positions 5 and 7, respectively. The sign of the local dihedral angle (LDA) has been defined as follows:

$$\mathrm{sign}(LDA) = \mathrm{sign}(-\mathbf{x}_{ii} \cdot \mathbf{x}_{i,i+1} \times \mathbf{x}_{i+1,i+1}). \tag{2}$$

Supramolecular right and left-handed twists are associated with positive and negative values of $k_{i,i+1}^l$, respectively.

The time series of statistical observables have been considered as composed of two terms, i.e., for an observable A at the timestep t_s we write

$$A(t_s) = A(t_s)_{tw} + A(t_s)_{\mathrm{fluct}}, \tag{3}$$

where $A(t_s)_{tw}$ has been calculated as a moving/block average of $A(t_s)$ over a *time window* (this varied from $tw = 100$ to $tw = 1000$ timesteps for different observables as can be seen from Section 3):

$$A(t_s)_{tw} = \begin{cases} \frac{1}{t_s}\sum_{j=1}^{j=s} A(t_j) & \text{if } t_s < tw, \\ \frac{1}{tw}\sum_{j=s-tw}^{j=s} A(t_j) & \text{if } tw \geqslant t_s \leqslant N - tw, \\ \frac{1}{N-t_s}\sum_{j=s}^{j=N} A(t_j) & \text{if } t_s > N - tw, \end{cases} \tag{4}$$

where $N = 20\,000$ is the total number of timesteps.

The pair distribution function $g(r)$ of the inter-strand distances has been considered as an additional structural parameter. This has been calculated by averaging of the quantity calculated at every timestep as follows:

$$g(r) = \frac{2}{L(M-2)(M-3)} \sum_{l=1}^{L} \sum_{i=2}^{M-2} \sum_{j=i+1}^{M-1} \delta(d_{ij}^l - r), \tag{5}$$

where the δ is the Kronecker symbol, $M = 20$ is the number of peptides in a layer, L is the number of the layers in the assembly. The inter-strand distance d_{ij}^l between peptides within the layer l is defined as

$$d_{ij}^l = \begin{cases} \frac{|C_\alpha^i(5) - C_\alpha^j(7)| + |C_\alpha^i(6) - C_\alpha^j(6)| + |C_\alpha^i(7) - C_\alpha^j(5)|}{3} & \text{if } |i-j| \text{ is odd}, \\ \frac{|C_\alpha^i(5) - C_\alpha^j(5)| + |C_\alpha^i(6) - C_\alpha^j(6)| + |C_\alpha^i(7) - C_\alpha^j(7)|}{3} & \text{if } |i-j| \text{ is even}, \end{cases} \tag{6}$$

where $C_\alpha^i(X)$ is the position of the C_α atom for residue number X within the ith strand. Similarly, the nearest-neighbor inter-strand distance is defined as

$$\mathsf{d} = \frac{1}{L(M-3)} \sum_{l=1}^{L} \sum_{i=2}^{M-2} d_{i,i+1}^l. \tag{7}$$

3. Results

The last 4 ns of all simulations under both SHBC and PBC-PME are the actual production runs during which the coordinates are collected every 0.2 ps (total timesteps $N = 20\,000$) and used for calculation of the

representative structures (MD simulations under SHBC) and for the sampling of the structural observables (MD simulations under both SHBC and PBC-PME) [30].

To check the consistency of the chiral parameters $\theta_i^l(n)$ we consider their time series (MD simulations under SHBC), firstly monitoring the sign of the angles and finding that, in all the systems, the large majority of the angles (see Table 2) have a positive sign (right-handed twist [21]). Moreover we observe that, in trial simulations of tapes composed of peptides made from D-amino acids, the vast majority of the angles acquire negative values (left-handed twist [21]) (data not shown). Therefore, having successfully verified the consistency of the chiral parameters $\theta_i^l(n)$, the quantity

$$\Theta = \frac{1}{L(M-2)} \sum_{l=1}^{L} \sum_{i=2}^{M-1} \sum_{n=2}^{8} \theta_i^l(n) \tag{8}$$

is taken as a measure of the *total helicity* of the single strand (molecular-scale chiral parameter).

A similar analysis has been carried out on the parameters $k_{i,i+1}^l$ with finding that all the local twist angles have a negative sign, which corresponds to a left-handed twist (data not shown). Therefore, the quantity

$$\mathsf{k} = \frac{1}{L(M-3)} \sum_{l=1}^{L} \sum_{i=2}^{M-2} k_{i,i+1}^l \tag{9}$$

is taken as the supramolecular-scale chiral parameter.

We obtain tape, ribbon and double ribbon representative structures by exploiting the following two-step numerical procedure. Firstly, the average ('iso middle') structure is calculated by using the least-square aligning algorithm within the GROMACS software [39–42]. Secondly, an 'annealing' procedure based on a local minimization of the potential energy, by using a steepest-descent algorithm [27,28], is performed for the purpose of removing possible steric (Lennard-Jones) clashes which have resulted from using the least-square algorithm.

Secondary structure validation is carried out calculating the Ramachandran plots [43] for each one of the six representative structures (data not shown). The plots show that the vast majority (98–100%) of the residues are in the upper-left quadrant, confirming thereby the β-sheet nature of the clusters.

The six representative structures generated from the MD simulations under SHBC are all of a chiral nature (see Figs. 1 and 2). On the one hand, systems TP1 and TP2 resemble left-handed helical tapes with a regular twist and bend (cylindrical curvature). On the other hand, systems RP1, RP2, DP1 and DP2 resemble circular left-handed helicoids with a regular twist and a negligible bending (saddle-like curvature) [47]. While the twist of all the assemblies is related to the chiral nature of the strands as well as to the interactions between neighboring strands (see Section 1), the finite bend in the single tape systems is due to different chemical nature of their two sides and the resulting asymmetry in the surface forces [1].

Both the (meta)stability and the equilibration of the clusters have been analyzed by calculating both the root mean-square deviation (RMSD) from the representative structures together with the power spectrum of the RMSD in the frequency space.

Table 2
Percentage of positive values in the time series of parameters $\theta_i^l(n)$

Time series of $\theta_i^l(n)$	
System	$\%\theta_i^l(n)>0$
TP1	100%
TP2	>99.9%
RP1	>99.9%
RP2	96.4%
DP1	>99.9%
DP2	77.5%

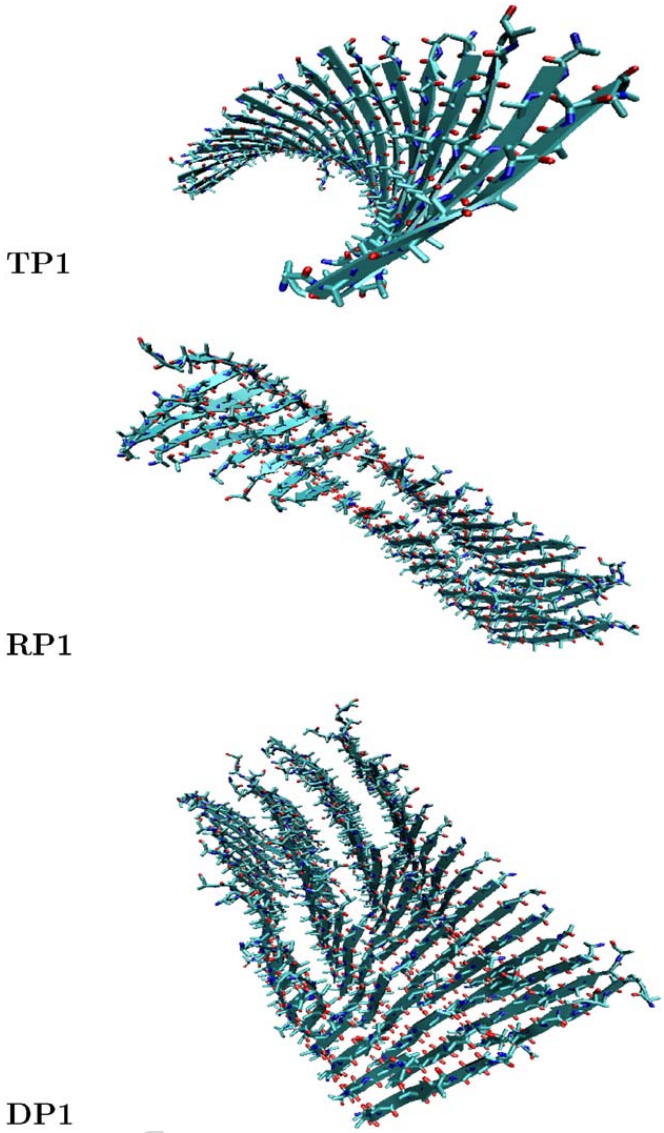

Fig. 1. Representative structures of clusters formed by peptide P_{11}-I obtained from molecular dynamics simulations under spherical boundary conditions (see Section 3). Side-chains are not shown for better clarity.

Plots of the smoothed quantity $RMSD(t_s)_{1000}$ for the tape clusters TP1 and TP2 (see Fig. 3) show persistent fluctuations from the average value. The nature of these fluctuations can be well explained by the power spectra which both consist of several vibrational modes above the significance level. With the increase of the complexity of the systems, i.e., while considering the ribbons and the double ribbons, the fluctuations above the average RMSD decrease and the power spectra display one to two significant low-frequency vibrational modes (see Figs. 4 and 5).

Next, we calculate time series of the fluctuations for the RMSD and for the chiral parameters Θ and k as

$$A(t_s)_{\text{fluct}} = A(t_s) - A(t_s)_{tw}, \tag{10}$$

where $tw = 1000$ for the RMSD and $tw = 100$ for the chiral parameters Θ and k. The results for the standard deviation of $A(t_s)_{\text{fluct}}$ are shown in Table 3 (data from PBC-MD simulations are given in parentheses).

From the data in Figs. 3–5 and in Table 3, one can clearly see that the stability monotonically increases with the complexity of the structures, i.e., from tape to ribbon and from ribbon to double ribbon. This tendency is of a similar nature for both peptides P_{11}-I and P_{11}-II and can be observed in the data from MD simulations

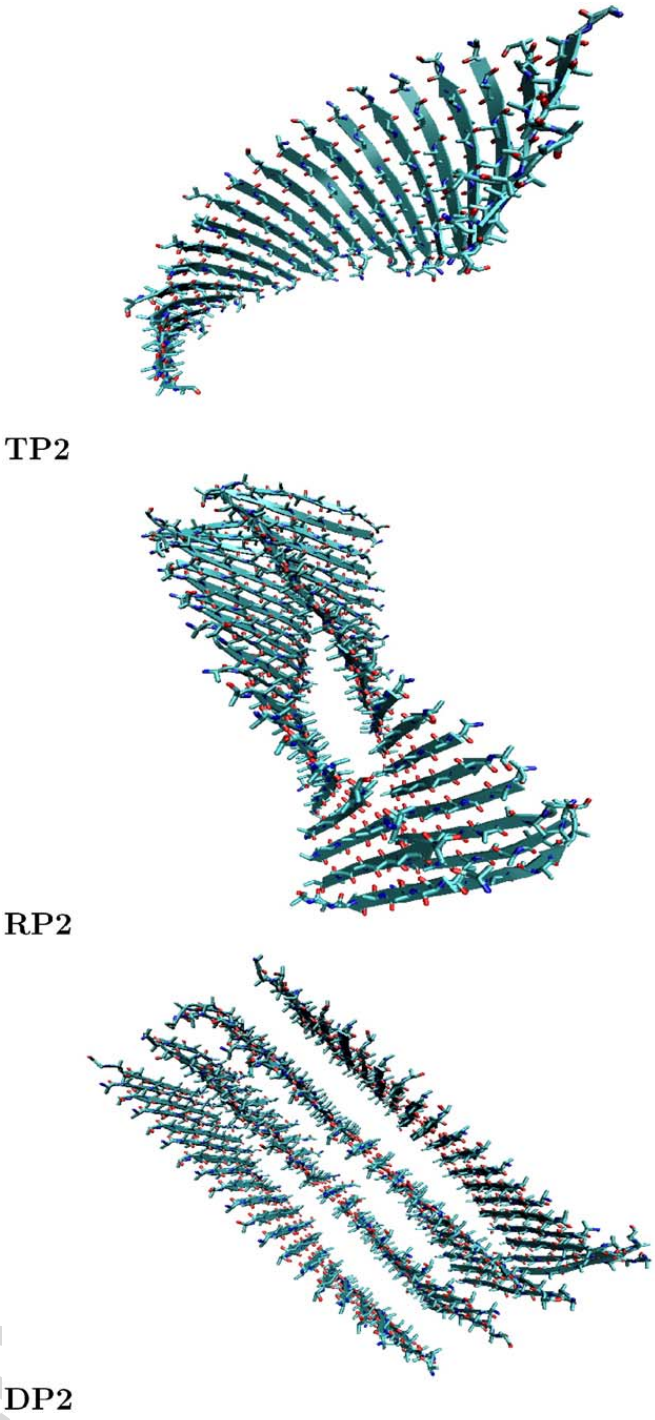

Fig. 2. Representative structures of clusters formed by peptide P_{11}-II obtained from molecular dynamics simulations under spherical boundary conditions (see Section 3). Side-chains are not shown for better clarity.

under both SHBC and PBC-PME. Furthermore, the structures generated from SHBC simulations are somewhat more rigid than the corresponding ones generated from PBC-PME simulations. This can be clearly seen from the time series of the quantity $RMSD(t_s)_{1000}$ (Figs. 3–5) and from the fluctuations of the RMSD and of the chiral parameters Θ and k in Table 3.

For completing our analysis on the stability of the clusters we plot in Figs. 3–5 the time average of the pair distribution function of the inter-strand distances (Eq. (5)). The functions exhibit a series of well defined

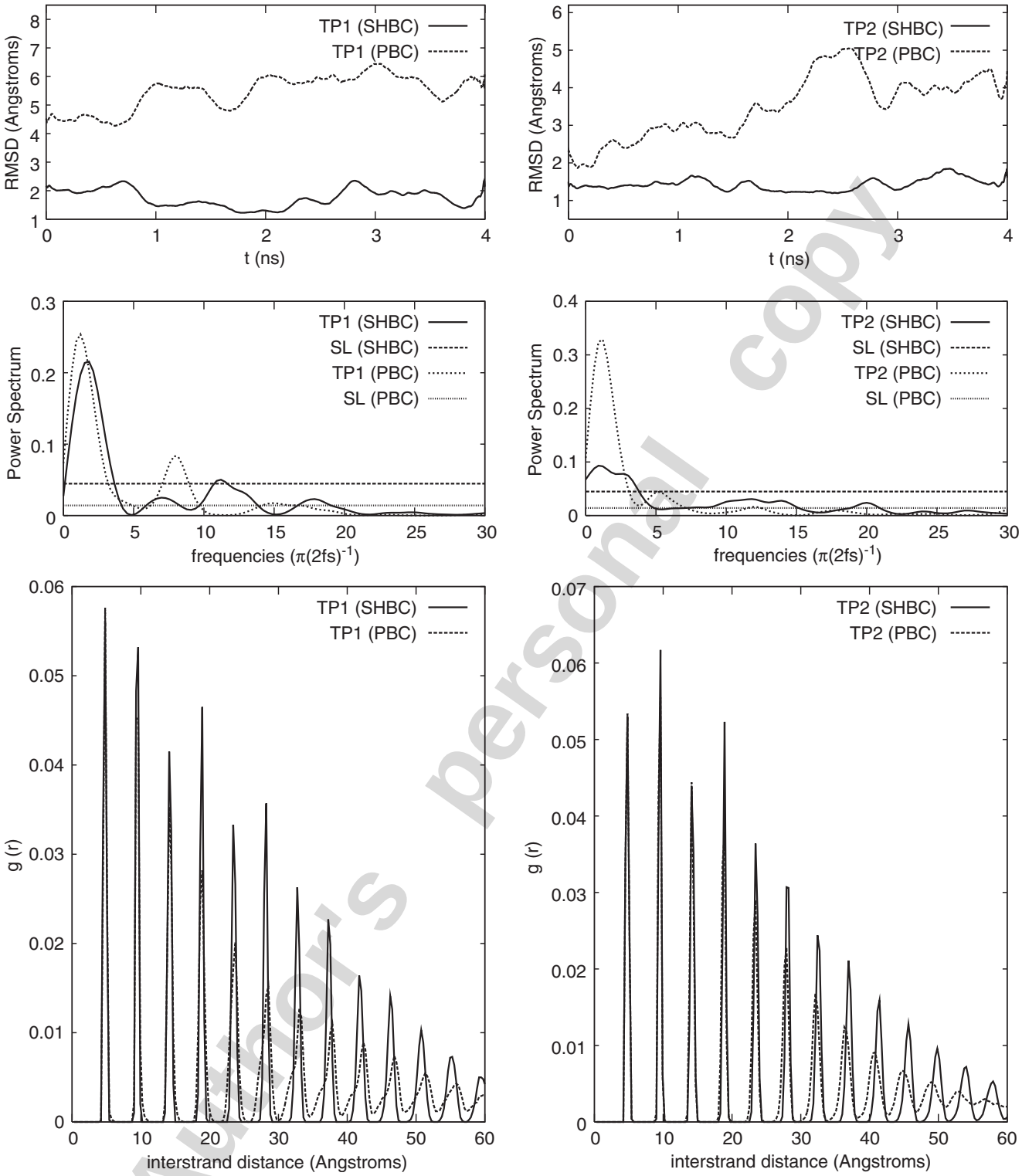

Fig. 3. Left: System TP1. Right: System TP2. Top: Times series, $\langle A_{t_i}\rangle_{1000}$, for the root mean-square deviation RMSD from representative structure. Middle: power spectrum for RMSD, $\mathrm{SL} = 2/\sqrt{N}$ is the significance level, N is the number of time steps. Bottom: time averaged pair distribution function $g(r)$ of the inter-strand distance (see Eqs. (5), (6)).

narrow peaks for all structures indicating solid-like order within tapes, ribbons and double ribbons. Of all these, tapes have the least of long-range order as evidenced by the lack of clear separation between the peaks at large separations, which is however much enhanced in ribbons and double ribbons. The narrowness of the

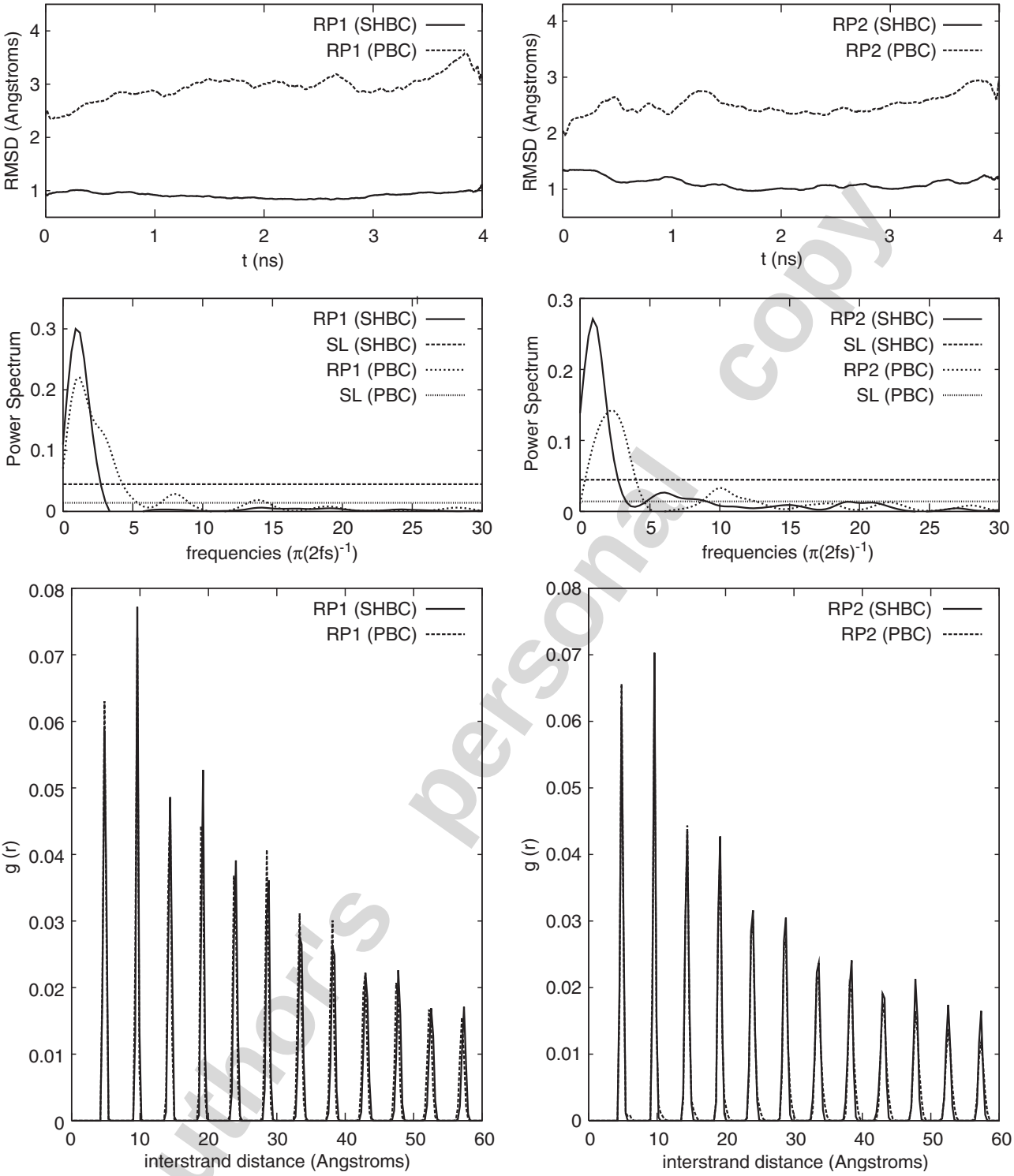

Fig. 4. Left: System RP1. Right: System RP2. Top: Times series, $\langle A_{t_i} \rangle_{1000}$, for the root mean-square deviation RMSD from representative structure. Middle: power spectrum for RMSD, SL $= 2/\sqrt{N}$ is the significance level, N is the number of time steps. Bottom: time averaged pair distribution function $g(r)$ of the inter-strand distance (see Eqs. (5), (6)).

peaks is the consequence of well-defined inter-strand distances. The lack of long-range order in tapes is more evident in PBC-PME simulations than in SHBC simulations, while for ribbons and double ribbons there is no real difference between the $g(r)$'s plots generated under PBC and SHBC.

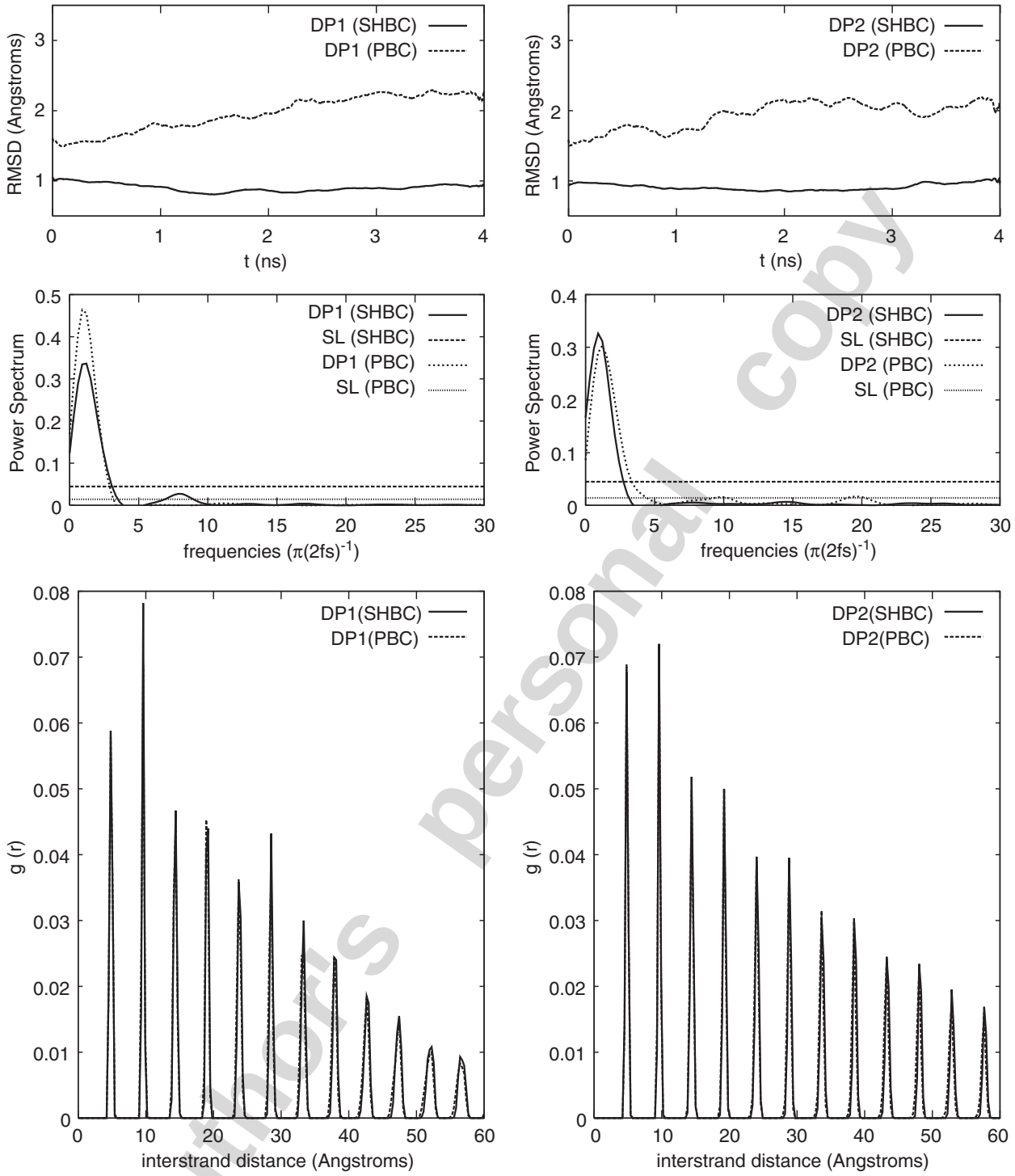

Fig. 5. Left: System DP1. Right: System DP2. Top: Times series, $\langle A_{t_i} \rangle_{1000}$, for the root mean-square deviation RMSD from representative structure. Middle: power spectrum for RMSD, SL $= 2/\sqrt{N}$ is the significance level, N is the number of time steps. Bottom: time averaged pair distribution function $g(r)$ of the inter-strand distance (see Eqs. (5), (6)).

The time averaged values (over the MD production runs) of the chiral parameters Θ and k and of the nearest-neighbor inter-strand distance d are reported in Table 4 (data from PBC-PME MD simulations are given in parentheses). The values for the pitch wave number k and for the nearest-neighbor inter-strand distance d obtained from the simulations are consistent with the known experimental results [1].

Table 3
Standard deviation $\sigma(A(t_s)_{\text{fluct}})$ obtained from MD simulations under SHBC for the root mean-square deviation (RMSD) and for the chiral parameters Θ (*total helicity* of the single strand, molecular-scale chiral parameter) and k (pitch wave number, supramolecular-scale chiral parameter)

$\sigma(A(t_s)_{\text{fluct}})$			
System	RMSD (Å)	Θ (deg.)	k (deg.)
TP1	0.23(0.36)	3.14(7.91)	0.30(0.57)
RP1	0.05(0.15)	1.98(3.43)	0.23(0.33)
DP1	0.03(0.09)	1.34(1.78)	0.17(0.22)
TP2	0.17(0.41)	3.21(6.25)	0.28(0.55)
RP2	0.06(0.15)	2.03(3.51)	0.23(0.51)
DP2	0.04(0.12)	1.37(1.80)	0.19(0.23)

In parentheses: averaged values and standard deviations obtained from MD simulations under PBC (PME).

Table 4
Time averaged values and standard deviations σ obtained from MD simulations under SHBC for the parameters Θ (*total helicity* of the single strand, molecular-scale chiral parameter), k (pitch wave number, supramolecular-scale chiral parameter) and for the nearest-neighbor inter-strand distance d

Parameters Θ, k and d						
System	Θ (deg.)	σ_Θ	k (deg.)	σ_k	d (Å)	σ_d
TP1	120.4(162.8)	9.8(12.0)	−8.6(−13.0)	0.6(0.9)	4.8(4.8)	<0.1(<0.1)
RP1	59.7(90.1)	2.7(4.8)	−4.3(−6.4)	0.3(0.4)	4.8(4.8)	<0.1(<0.1)
DP1	46.9(53.9)	2.4(3.3)	−2.3(−3.4)	0.2(0.4)	4.8(4.8)	<0.1(<0.1)
TP2	105.3(126.6)	5.2(8.6)	−8.1(−10.6)	0.4(0.9)	5.0(5.0)	<0.1(<0.1)
RP2	61.3(80.5)	3.4(4.8)	−5.7(−7.0)	0.3(0.5)	4.9(4.9)	<0.1(<0.1)
DP2	29.6(37.3)	1.9(4.4)	−1.7(−2.1)	0.2(0.3)	4.9(4.9)	<0.1(<0.1)

In parentheses: averaged values and standard deviations obtained from MD simulations under PBC (PME).

Firstly, experimental values for the pitch wave number k have been calculated for tapes, ribbons and fibrils from TEM micrographs analysis [1]. It was found that single and double tapes formed by the peptide P_{11}-I both possess the pitch wave number $k = -3^\circ$, while fibrils formed by the peptide P_{11}-II possess the pitch wave number $k = -1^\circ$. These experimental values do not seem to be very accurate as their percentage error goes from 25% to 50%. Nevertheless, they are the only reliable data, which can be currently used for comparison and validation of theoretical and computational studies on the chiral properties of clusters formed by the peptides P_{11}-I and P_{11}-II.

Secondly, X-ray diffraction data [1] reveal a value for the nearest-neighbor inter-strand distance of $d = 4.7$ Å in all structures. These data are consistent with the expected nearest-neighbor inter-strand distance in a β-sheet ($d = 4.7-4.8$ Å).

There are some differences between the values for Θ and k calculated from MD simulations under SHBC and PBC-PME. Those differences decrease from tape to ribbon, and to double ribbon, for both P_{11}-I and P_{11}-II-based systems.

As there are no reliable experimental data for the validation of the two chiral parameters Θ and k (limited precision for k and no experimental data at all for Θ), and as both Ewald sum and spherical cut-off methods have their drawbacks and artifacts [33,36–38], it is difficult to say which one produces the best data. However, we can notice that, regarding k, the values obtained in MD simulations under SHBC are closer to the current experimental values.

The *transfer* of chirality from the molecular scale of the β-strands to the greater supramolecular scale of the β-tapes, ribbons and double ribbons can be clearly seen from the results in Table 4. Indeed, the sign and the

magnitude of the helical deformation of the single strands (as indicated by the value of Θ) directly relates to the handedness and the magnitude of the macroscopic twist (as indicated by the pitch wave number k).

The decrease of the parameters Θ and $|\mathsf{k}|$ from tape to ribbon and from ribbon to double ribbon can be explained by observing that, despite of the intra-molecular origin of chirality, the conformation of the single strands within a cluster depends also on their interactions with the neighboring strands. As the magnitude of these short-ranged cohesive interactions increases with the complexity of the cluster, so the helical deformation of the single strand decreases.

While the decrease of the parameters Θ and $|\mathsf{k}|$ from tape to ribbon and from ribbon to double ribbon cannot be fully confirmed experimentally (due to the lack of high resolution data) it has been also observed in previous MD simulations (on tapes and ribbons only) on P_{11}-I and P_{11}-II [25].

A more detailed analysis of both the molecular and intermolecular chiral parameters is given in Figs. 6 and 7. We plot the potential of the mean force (PMF) for Θ and k, respectively.

The PMF for a reaction coordinate ξ is calculated as

$$PMF(\xi) = -\ln(p(\xi)) + \ln(p_{max}(\xi)), \tag{11}$$

where $p(\xi)$ is the probability distribution for ξ and $p_{max}(\xi)$ is the most probable value of ξ.

The combined analysis of Tables 3 and 4, and of the *PMF* plots (Figs. 6 and 7) leads us to the following observations regarding the chirality of the clusters:

(1) The two different treatments of the long-range ES forces used in our study produce different results for both the parameters Θ and k.
(2) MD simulations under SHBC give smaller values for both Θ and $|\mathsf{k}|$ if compared to MD simulations under PBC.
(3) Both the standard deviations in Tables 3 and 4, and the width of the *PMF* profile at $1K_BT$ (horizontal line in Figs. 6 and 7) confirm that MD simulations under SHBC produce more 'frustrated' structures as far as regards the chiral parameters.

For understanding the origin of those differences we plot in Figs. 8–12 the probability distributions of the Ramachandran angles Φ and Ψ for the different amino acids in P_{11}-II clusters.

On the one hand, conformations of Arginine, Glutamic acid and Glutamine (in Figs. 8–10, respectively) show clear differences between SHBC and PBC simulations on the distributions of the Ramachandran angle Φ. A similar behavior has been found in P_{11}-I clusters (data not shown). On the other hand, Phenylalanine and Tryptophan (in Figs. 11 and 12, respectively) do not seem to be affected by the two different treatments of the long-range ES forces. In our opinion, such 'persistence' in different ES treatments is due to two important facts: (1) they carry no net charge; (2) they have high propensity to be in the β-sheet conformation [44,45].

In addition, it can be noted that Glutamine residues have a tendency to be also in PolyProline-II conformation ($\Phi = -78^\circ$, $\Psi = 146^\circ$) [46] in both SHBC and PBC simulations. In our simulations, this tendency is common to both P_{11}-I (data not shown) and P_{11}-II, and it decreases with increasing the complexity of the clusters. The high intrinsic propensity for Glutamine to be in PolyProline-II conformation has been observed in a computational analysis over a database of (274) non-homologous polypeptide chains which possess regions forming PolyProline-II structures [46].

For completing our investigation on the effect of the range of forces on the stability and on the geometrical properties of the clusters, we run, for systems RP1 and RP2, additional 1 ns MD simulations under SHBC with different cut-offs for non-bonded interactions, namely 5.8 and 13 Å. The results obtained for the chiral parameters Θ and k are displayed in Table 5. Standard deviations (as a measure of stability) seem to increase with increasing cut-offs, while the average values do not seem to change considerably.

4. Conclusion

In this paper, we have presented the results from MD simulations, of β-tapes, ribbons and double ribbons formed by the synthetic de novo oligopeptides P_{11}-I and P_{11}-II in solution.

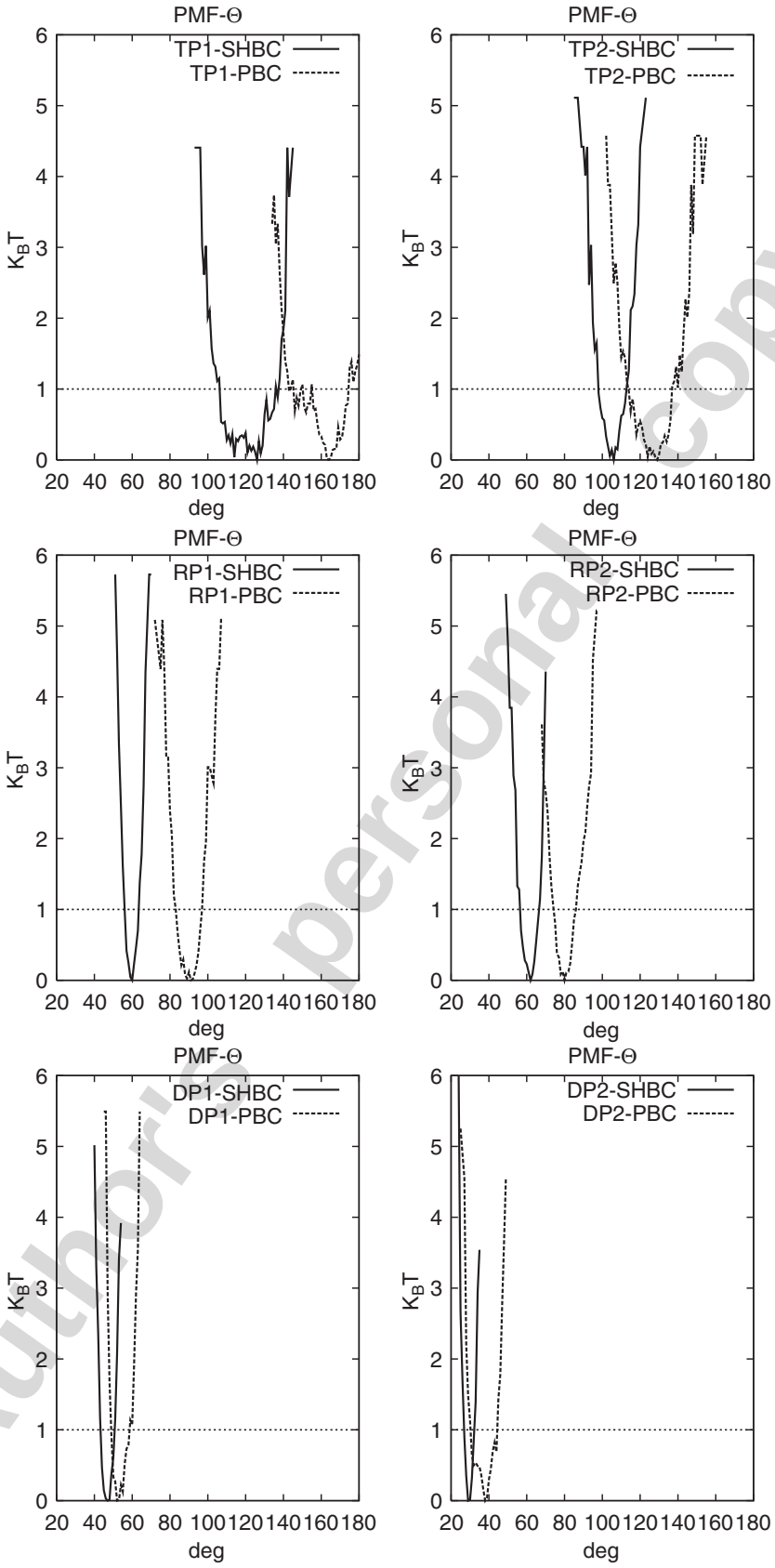

Fig. 6. Potential of the mean force for the molecular chiral parameter Θ. SHBC: MD simulations under spherical harmonic boundary conditions with force-shifted spherical cutoff. PBC: MD simulations under periodic boundary conditions with particle mesh Ewald. Top: systems TP1 (left) and TP2 (right), Middle: systems RP1 (left) and RP2 (right), Bottom: systems DP1 (left) and DP2 (right).

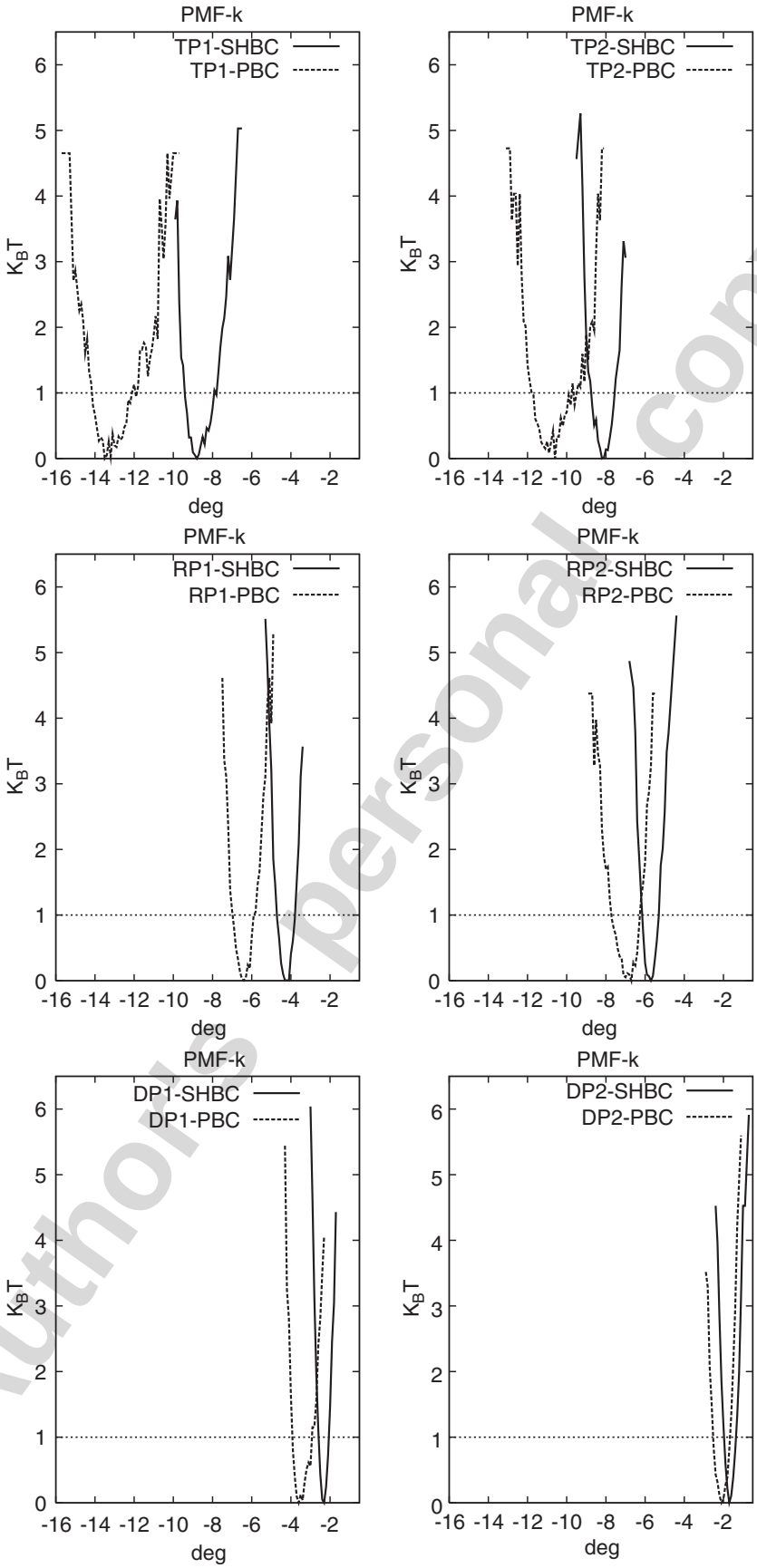

Fig. 7. Potential of the mean force for the molecular chiral parameter k. SHBC: MD simulations under spherical harmonic boundary conditions with force-shifted spherical cutoff. PBC: MD simulations under periodic boundary conditions with particle mesh Ewald. Top: systems TP1 (left) and TP2 (right), Middle: systems RP1 (left) and RP2 (right), Bottom: systems DP1 (left) and DP2 (right).

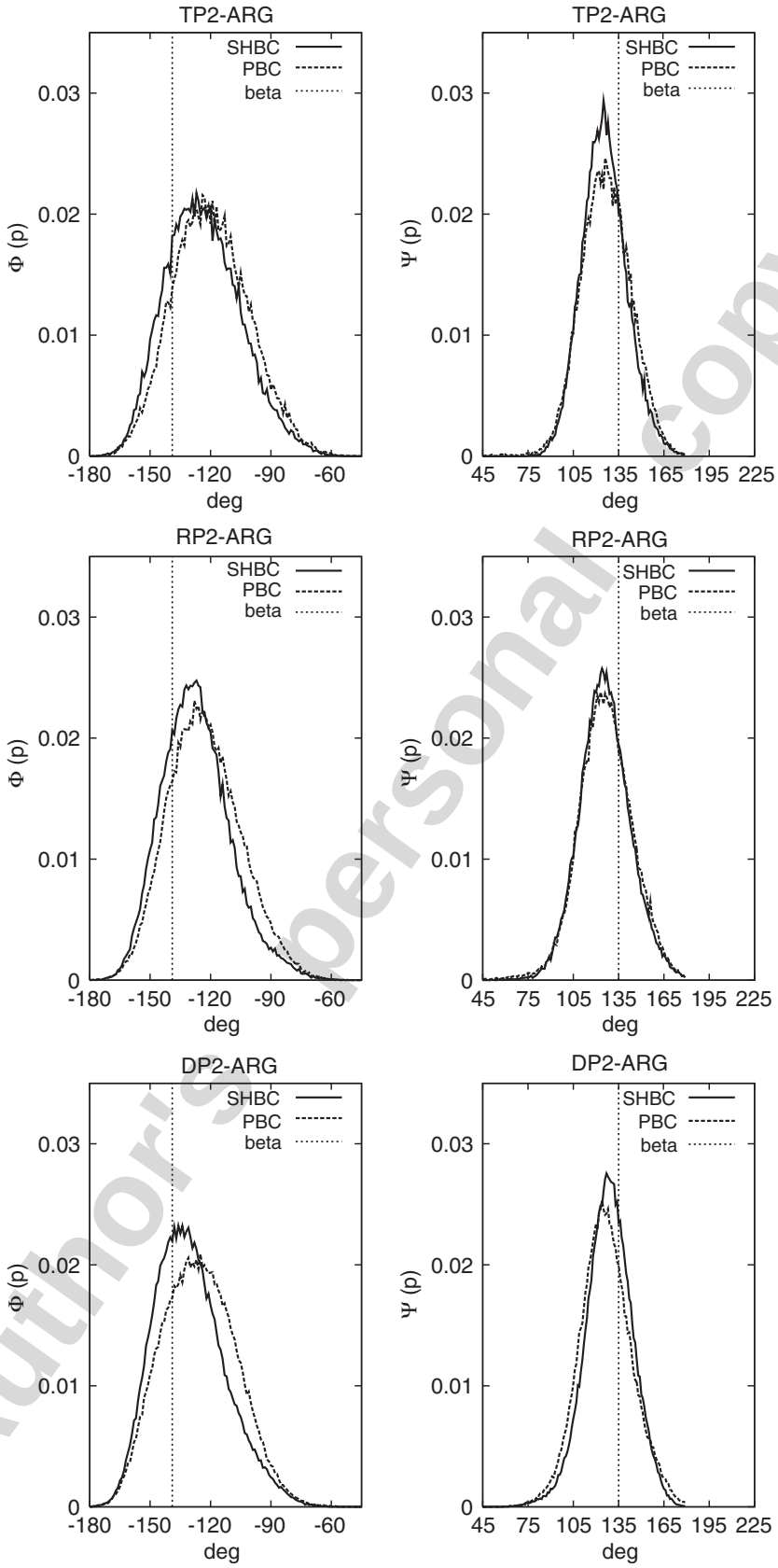

Fig. 8. Probability distributions of the dihedral angles Φ (left) and Ψ (right) for aminoacid ARG obtained from MD simulations. SHBC: MD simulations under spherical harmonic boundary conditions with force-shifted spherical cutoff. PBC: MD simulations under periodic boundary conditions with particle mesh Ewald. Beta: (vertical line) fully extended antiparallel β-sheet. Top: system TP2, Middle: system RP2, Bottom: system DP2.

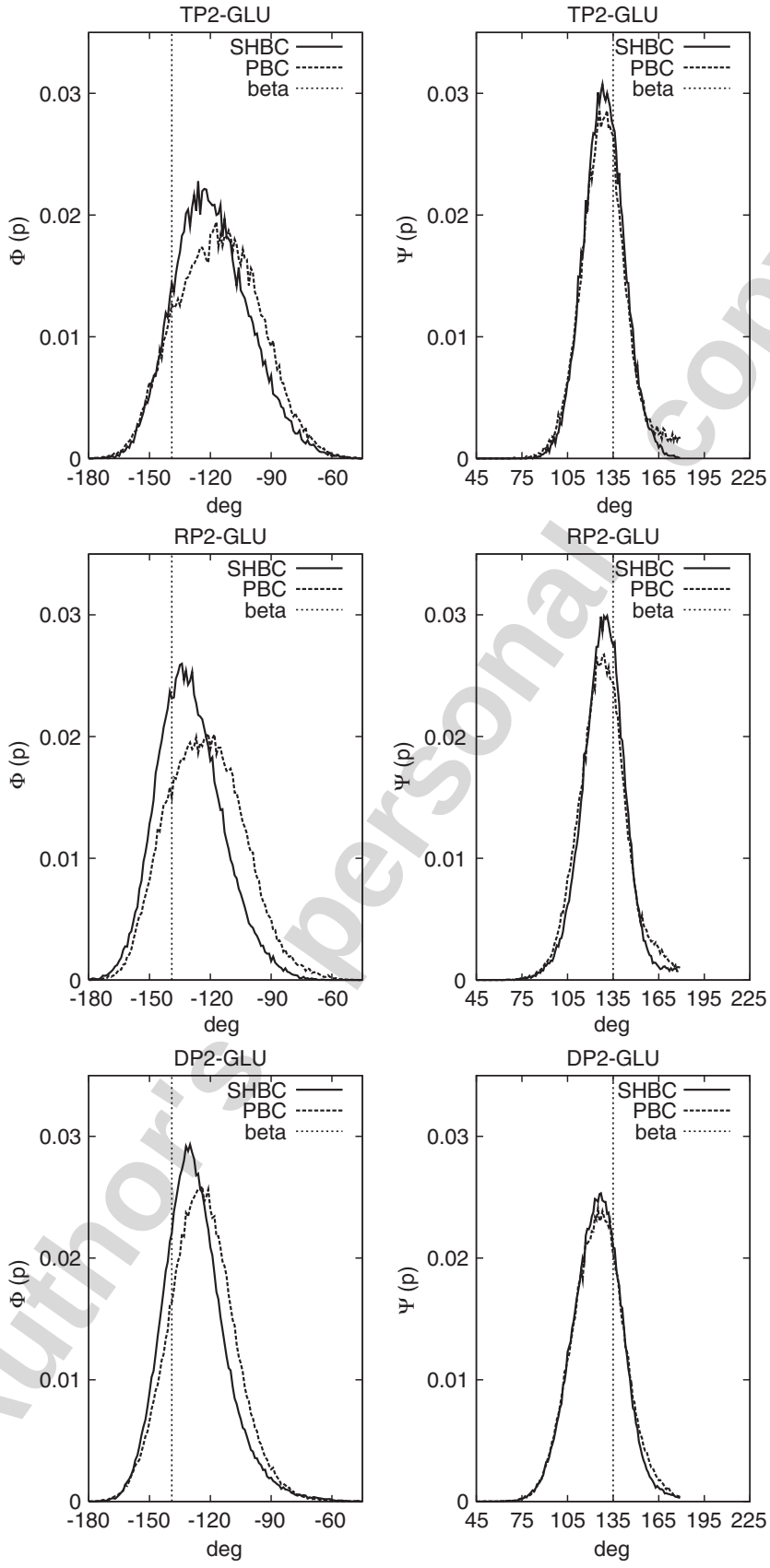

Fig. 9. Probability distributions of the dihedral angles Φ (left) and Ψ (right) for aminoacid GLU obtained from MD simulations. SHBC: MD simulations under spherical harmonic boundary conditions with force-shifted spherical cutoff. PBC: MD simulations under periodic boundary conditions with particle mesh Ewald. Beta: (vertical line) fully extended antiparallel β-sheet. Top: system TP2, Middle: system RP2, Bottom: system DP2.

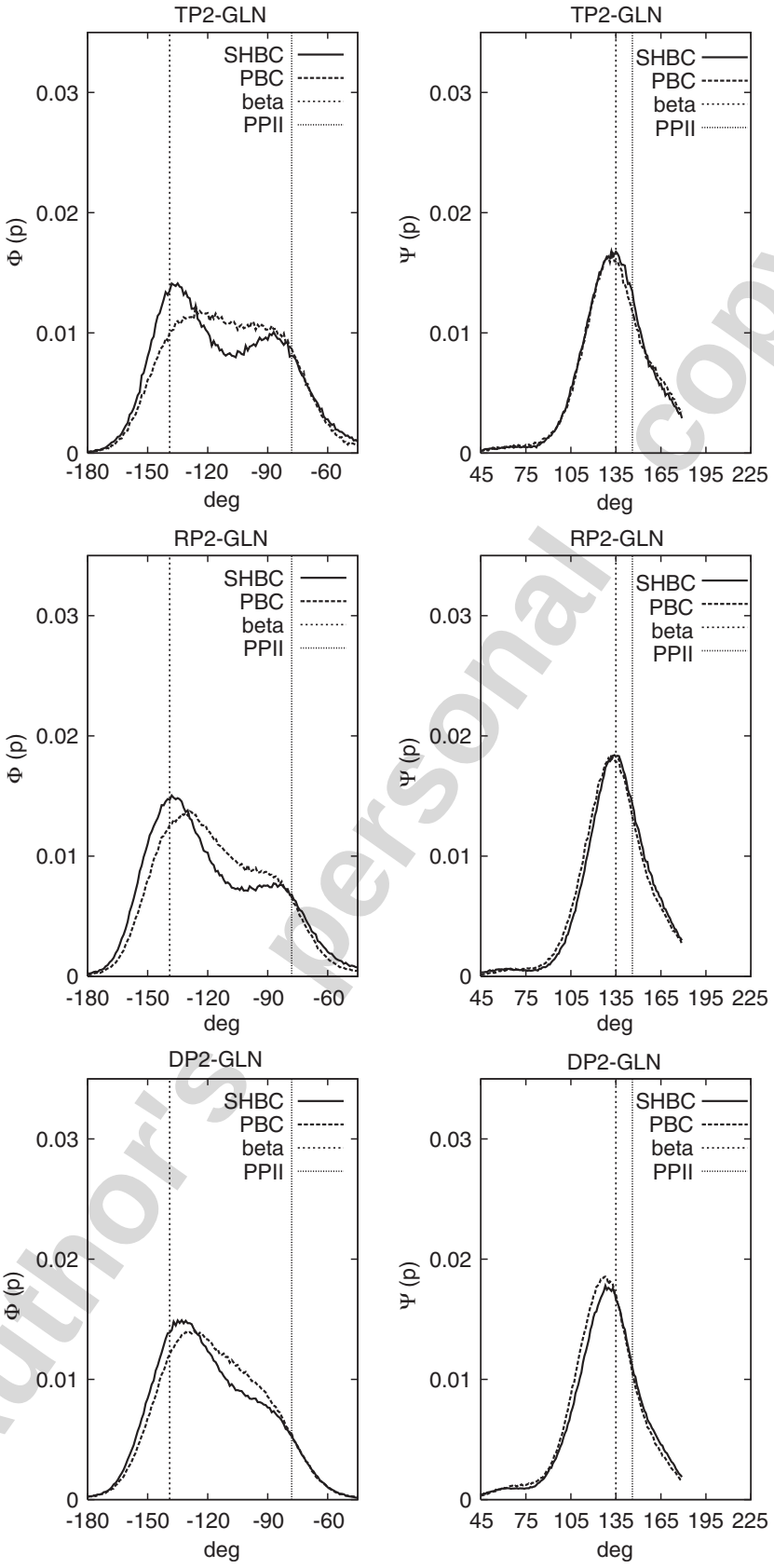

Fig. 10. Probability distributions of the dihedral angles Φ (left) and Ψ (right) for aminoacid GLN obtained from MD simulations. SHBC: MD simulations under spherical harmonic boundary conditions with force-shifted spherical cutoff. PBC: MD simulations under periodic boundary conditions with particle mesh Ewald. Beta: (vertical line) fully extended antiparallel β-sheet. PPII: polyproline-II conformation. Top: system TP2, Middle: system RP2, Bottom: system DP2.

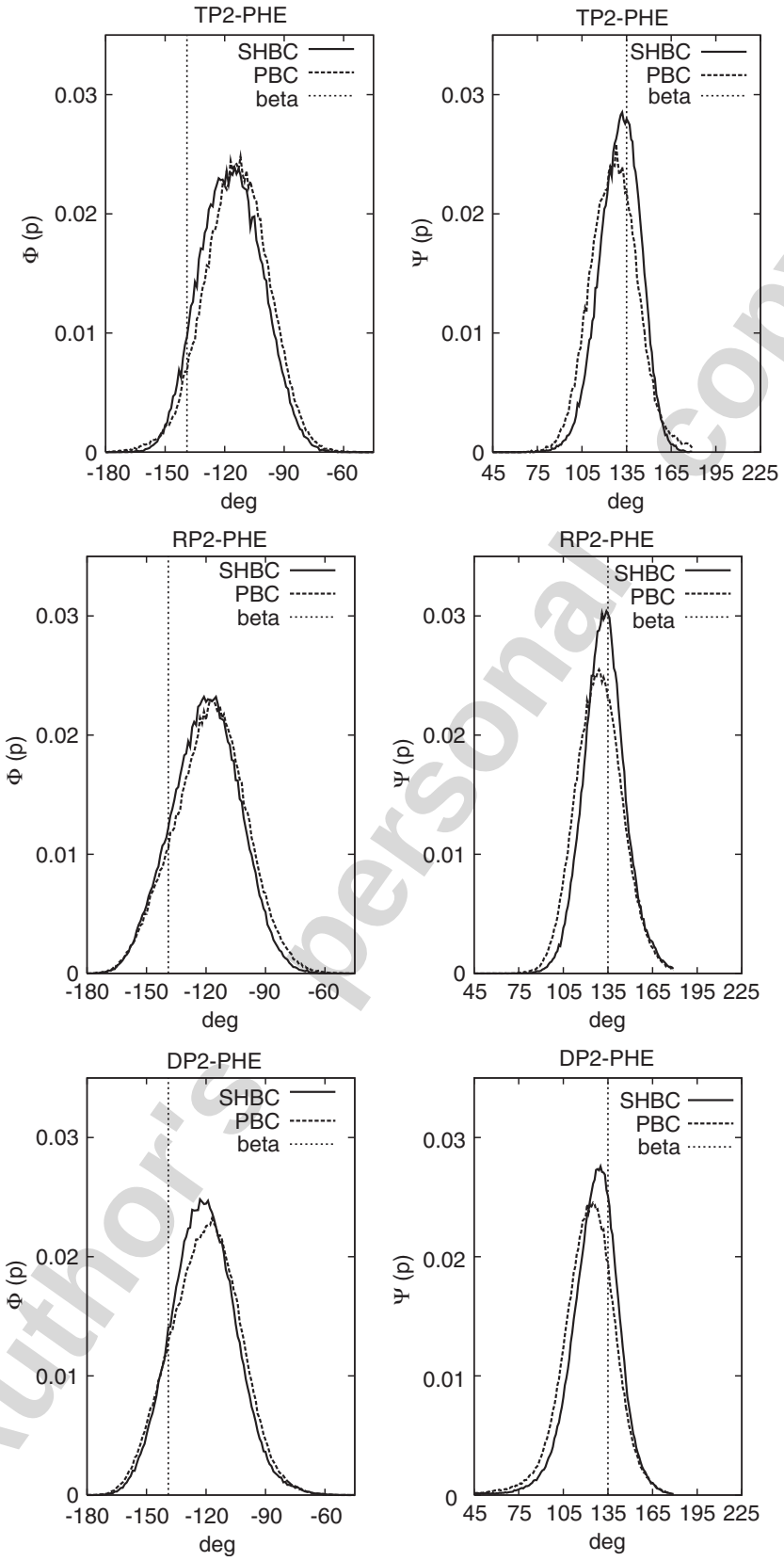

Fig. 11. Probability distributions of the dihedral angles Φ (left) and Ψ (right) for aminoacid PHE obtained from MD simulations. SHBC: MD simulations under spherical harmonic boundary conditions with force-shifted spherical cutoff. PBC: MD simulations under periodic boundary conditions with particle mesh Ewald. Beta: (vertical line) fully extended antiparallel β-sheet. Top: system TP2, Middle: system RP2, Bottom: system DP2.

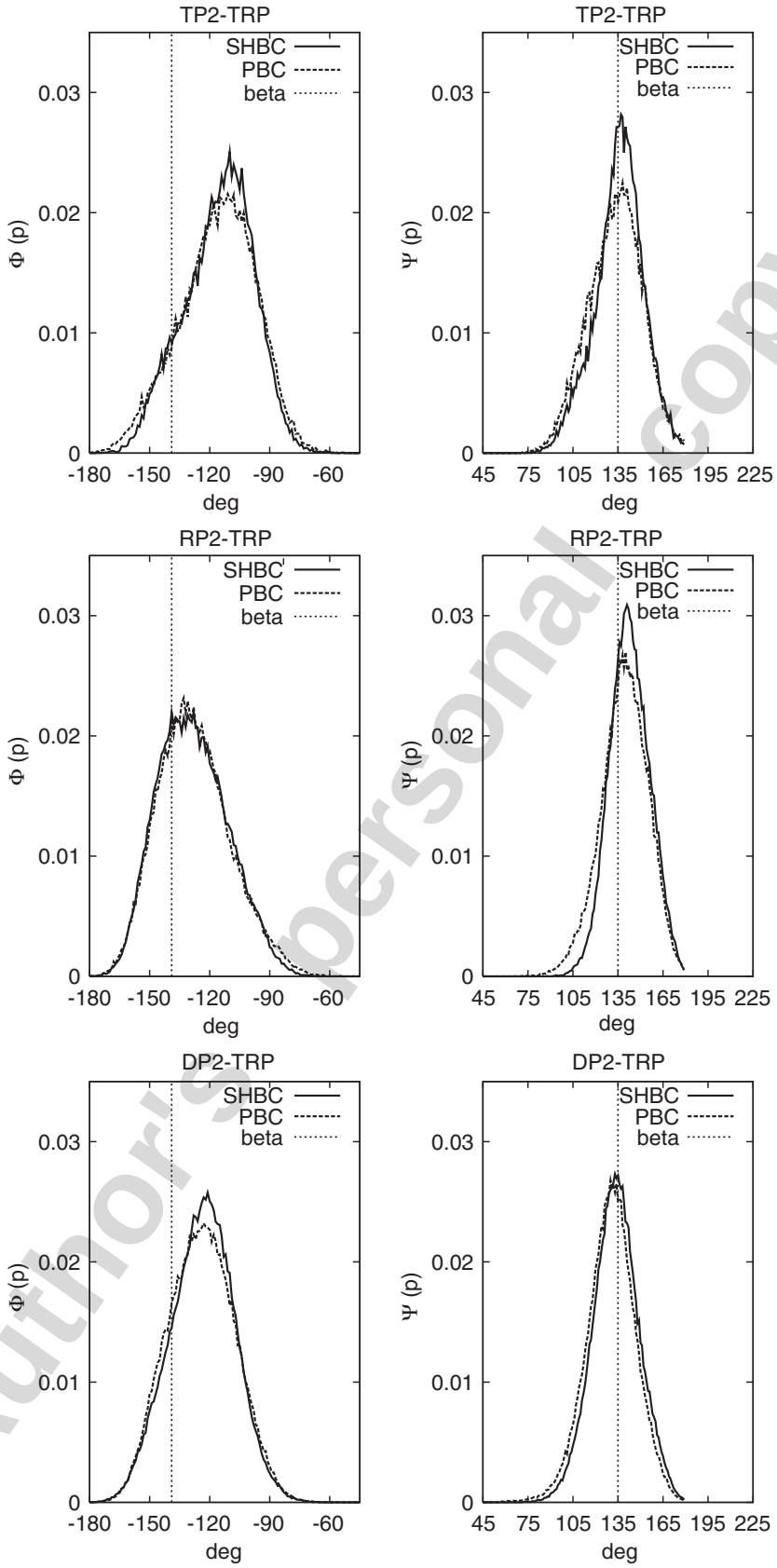

Fig. 12. Probability distributions of the dihedral angles Φ (left) and Ψ (right) for aminoacid TRP obtained from MD simulations. SHBC: MD simulations under spherical harmonic boundary conditions with force-shifted spherical cutoff. PBC: MD simulations under periodic boundary conditions with particle mesh Ewald. Beta: (vertical line) fully extended antiparallel β-sheet. Top: system TP2, Middle: system RP2, Bottom: system DP2.

Table 5
Time averaged values and standard deviations σ for the chiral parameters Θ and k, obtained from additional 1 ns molecular dynamics runs (under SHBC) of ribbons

Cut-off and chiral parameters					
System	Cut-off (Å)	Θ (deg.)	σ_Θ	k (deg.)	σ_k
RP1	5.0	59.4	2.5	−4.1	0.2
RP1	8.0	61.0	3.0	−4.3	0.3
RP1	13.0	61.1	3.3	−4.4	0.3
RP2	5.0	59.4	2.5	−4.9	0.2
RP2	8.0	61.1	3.6	−5.3	0.3
RP2	13.0	69.4	3.8	−5.8	0.4

Three different values were used for the spherical cut-off of both the Lennard-Jones potential and the Coulombic potential.

Two different methods for the treatment of the electrostatic interactions and the boundary conditions have been used: (see Sections 2 and 3): the (force-shifted) spherical cut-off method under SHBC (MD–SHBC) and the particle mesh Ewald method under PBC (MD–PME).

The spherical cut-off method and the particle mesh Ewald method give us qualitatively similar results in the calculation of the structural observables.

All the supramolecular structures are shown to be stable during dozens of nanosecond long simulations with explicit water molecules. The inter-strand radial distribution functions of these structures contain series of sharp peaks, indicating solid-like order within and thus there are well-defined inter-strand separations. The structures become more rigid with their increased complexity on going from tapes to ribbons (double tapes) and to double ribbons.

A clear connection has been established between the molecular degree of chirality of β-strands, Θ, and the supramolecular chirality of the clusters (expressed by the pitch wave number k). This connection is similar for both considered oligopeptides P_{11}-I and P_{11}-II, despite of the differences in their primary structures. The values for pitch wave number k and the inter-strand distance d calculated here agree quite well with the known experimental data.

It is not very clear which method for the treatment of the boundary conditions and the electrostatic forces worked better in our computer studies as the lack of high-quality structural data from experiments does not allow one to have a perfect validation of the calculation results. Nevertheless, one could make the following comments.

We observe from Table 5 and from comparison between MD–SHBC and MD–PBC simulations that the stability of the clusters depends mainly on short-range cohesive forces. In fact, when longer-range forces are considered (first increasing the value of the cutoff in MD–SHBC simulations and then running MD–PBC simulations) the fluctuations along the average values of the main structural parameters increase significantly.

Consequently, the MD–SHBC simulations generate more rigid structures than the MD–PME simulations. This increased rigidity may be also related to the finite size of the water sphere (which may limit the motion of the cluster and enhance the rigidity somewhat).

Importantly, we should stress out that this dynamical frustration may reproduce the "natural frustration" within much larger clusters observed in TEM micrographs, from which the chiral parameter k is extracted. Indeed, the MD–SHBC simulations seem to give a better agreement with the experiments. This last result should be taken into consideration if one wants to access longer MD time scales since the computational 'cost' of the spherical cutoff methods is intrinsically lower than the one of the Ewald-related techniques.

Acknowledgments

The authors would like to thank Professor Neville Boden and Dr Amalia Aggeli, as well as our colleagues Dr Ronan Connolly and Dr Nikolaj Georgi for useful discussions. Support from the IRCSET basic research

Grant SC/02/226 is also gratefully acknowledged. One of us (M.V.F.) is grateful to the Project HPC-EUROPA (RII3-CT-2003-506079), with the support of the European Community—Research Infrastructure Action under the FP6 'Structuring the European Research Area' Programme and to the SFI/HEA Irish Centre for High-End Computing (ICHEC).

References

[1] A. Aggeli, I.A. Nyrkova, M. Bell, R. Harding, L.M. Carrick, T.C.B. McLeish, A.N. Semenov, N. Boden, Proc. Natl. Acad. Sci. USA 98 (2001) 11857–11862.
[2] S. Zhang, M. Altman, Reactive & Functional Polymers 41 (1999) 91–102.
[3] S. Zhang, Biotechnology Advances 20 (2002) 321–339.
[4] S. Zhang, D.M. Marini, W. Hwang, S. Santoso, Curr. Opin. Chem. Biol. 6 (2002) 865–871.
[5] J. Kisiday, M. Jin, B. Kurz, H. Hung, C. Semino, S. Zhang, A.J. Grodzinsky, Proc. Natl. Acad. Sci. USA 99 (2001) 9996–10001.
[6] T.C. Holmes, S. de Lacalle, X. Su, G. Liu, A. Rich, S. Zhang, Proc. Natl. Acad. Sci. USA 97 (2001) 6728–6733.
[7] D.G. Lynn, S.C. Meredith, J. Struct. Biol. 130 (2001) 153–173.
[8] C.K. Smith, L. Regan, Acc. Chem. Res. 270 (2001) 153–161.
[9] A. Aggeli, M. Bell, N. Boden, J.N. Keen, T.C.B. McLeish, I. Nyrkova, S.E. Ratdord, A.N. Semenov, J. Mater. Chem. 7 (7) (2001) 1135–1145.
[10] D.M. Marini, W. Hwang, D.A. Lauffenburger, S. Zhang, R.D. Kamm, Nano Lett. 2 (4) (2001) 295–299.
[11] W. Hwang, D.M. Marini, R.D. Kamm, S. Zhang, J. Chem. Phys. 118 (1) (2001) 389–3978.
[12] B. Ma, R. Nussinov, Proc. Natl. Acad. Sci. USA 99 (22) (2002) 14126–14131.
[13] A. Aggeli, M. Bell, N. Boden, J.N. Keen, P.F. Knowles, T.C.B. McLeish, M. Pithkeathly, S.E. Ratdord, Nature 386 (1997) 259–262.
[14] A. Aggeli, M. Bell, L.M. Carrick, C.W.G. Fishwick, R. Harding, P.J. Mawer, S. Radford, A.E. Strong, N. Boden, J. Am. Chem. Soc. 125 (2003) 9619–9628.
[15] C. Chothia, J. Mol. Biol. 75 (1973) 295–302.
[16] J.S. Richardson, Adv. Prot. Chem. 34 (1981) 167–339.
[17] D.H. Weatherford, F.R. Salemme, Proc. Natl. Acad. Sci. USA 76 (1) (1979) 19–23.
[18] F.R. Salemme, Prog. Biophys. Mol. Biol. 42 (1983) 95–133.
[19] A. Yang, B.J. Honig, Mol. Biol. 252 (1995) 366–376.
[20] L. Wang, T. O'Connell, A. Tropsha, J. Hermans, J. Mol. Biol. 262 (1995) 283–293.
[21] I.L. Shamowsky, G.M. Ross, R.J. Riopelle, J. Phys. Chem. B 104 (2000) 11296–11307.
[22] B.K. Ho, P.G.M. Curmi, J. Mol. Biol. 317 (2002) 291–308.
[23] J.V. Selinger, M.S. Spector, J.M. Schnur, J. Phys. Chem. B 105 (30) (2001) 7157–7169.
[24] G. Bellesia, M.V. Fedorov, Yu.A. Kuznetsov, E.G. Timoshenko, J. Chem. Phys. 122 (2005) 134901.
[25] C.W.G. Fishwick, A.J. Beevers, L.M. Carrick, C.D. Withehouse, A. Aggeli, N. Boden, Nano Lett. 3 (11) (2003) 1475–1479.
[26] HyperChem(TM), Hypercube, Inc., 1115 NW 4th Street, Gainesville, Florida 32601, USA.
[27] Kale, et al., J. Comp. Phys. 151 (1999) 283–312.
[28] J.C. Phillips, R. Rosemary Braun, W. Wang, J. Gumbart, E. Tajkhorshid, E. Villa, C. Chipot, R.D. Skeel, L. Kale, K. Schulten, J. Comput. Chem. 26 (2005) 1781–1802.
[29] A.D. MacKerell Jr., et al., J. Phys. Chem. B 102 (1998) 3586–3616.
[30] W. Humphrey, A. Dalke, K. Schulten, J. Molec. Graphics 14 (1) (1996) 33–38.
[31] H.C. Andersen, J. Comput. Phys. 52 (1983) 24–34.
[32] H.J.C. Berendsen, J.P.M. Postma, W.F. van Gunsteren, J. Hermans, J. Chem. Phys. 81 (1994) 3684–3690.
[33] D.A.C. Beck, R.S. Armen, V. Daggett, Biochemistry 44 (2005) 609–616.
[34] R. Garemyr, A. Elofsson, Proteins: Structure, Function, and Genetics 37 (1999) 417–428.
[35] S.W. de Leeuw, J.W. Perram, E.R. Smith, Proceedings of the Royal Society of London A 373 (1980).
[36] C. Sagui, T.A. Darden, Annu. Rev. Biophys. Biomol. Struct. 28 (1999) 155–179.
[37] A. Baumketner, J.J. Shea, Phys. Chem. B 109 (2005) 21322–21328.
[38] R.D. Lins, U. Rothlisberger, J. Chem. Theory Comput. 2006, CT0501699, ASAP article, Web release date: February 1, 2006.
[39] H.J.C. Berendsen, D. van der Spoel, R. van Drunen, Comp. Phys. Comm. 91 (1995) 43–56.
[40] E. Lindahl, B. Hess, D. van der Spoel, J. Mol. Mod. 7 (2001) 306–317.
[41] W. Kabsch, Acta Cryst. A 32 (1976) 922–923.
[42] W. Kabsch, Acta Cryst. A 34 (1978) 827–828.
[43] S.C. Lovell, P. de Bakker, et al., Proteins: Structure, Function & Genetics 50 (2002) 437–450.
[44] P.R. Bergethon, The Physical Basis of Biochemistry: The Foundations of Molecular Biophysics, Springer, New York, 1998, pp. 400–403.
[45] S. Hovmoller, T. Zhou, T. Ohlson, Acta Cryst. D 58 (2002) 768–776.
[46] B.J. Stapley, T.P. Creamer, Protein Science 8 (1999) 587–595.
[47] Pdb files of the representative structures are available on request.